Afshari, A., Dehghan, A., & Azarpeyvand, M. (2019). Novel Three-dimensional Surface Treatments for Trailing-Edge Noise Reduction. *AIAA Journal*. https://doi.org/10.2514/1.J058586

Novel Three-dimensional Surface Treatments for Trailing-Edge Noise Reduction

Abbas Afshari[1], Ali A. Dehghan[2]
Yazd University, Yazd, Iran

Mahdi Azarpeyvand[3]
University of Bristol, Bristol, United Kingdom, BS8 1TR

The present study is concerned with the experimental investigation of novel complex surface treatments as a passive trailing edge noise control technique. The proposed novel three-dimensional surface treatments, composed of a combination of finlets with different spacings and patterns, have shown better aeroacoustic performance than the standard two-dimensional treatments in terms of the reduction in the surface pressure power spectral density, the spanwise length-scale, eddy convection velocity and the trailing edge noise. Furthermore, the boundary layer flow measurements downstream of the surface treatments has provided some insight into the mechanisms through which three-dimensional surface treatments affect the flow structures, which can help improve the performance of such passive techniques for the suppression airfoil noise at source. The aerodynamic performance of the plates fitted with different surface treatments is also examined using the boundary layer velocity information. The results from this fundamental study can lead to the development of new generations of quieter airfoils with unconventional surface treatments.

Nomenclature

c = flat plate chord, m

C_D = drag coefficient

[1] School of Mechanical Engineering, Yazd University, PhD graduated
[2] School of Mechanical Engineering, Yazd University, Professor
[3]Department of Mechanical Engineering, University of Bristol, Reader in aeroacoustics, *m.azarpeyvand@bristol.ac.uk*
* A preliminary version of this paper was presented as Paper 2017-3499 at the 23rd AIAA/CEAS Aeroacoustics Conference, Denver, Colorado, 2016.

f	=	frequency, Hz
h (h^+)	=	finlet height, m (made dimensionless using wall units)
s (s^+)	=	finlet wall spacing, m (made dimensionless using wall units)
t	=	trailing edge thickness, m
u	=	streamwise velocity, m/s
U_c	=	convection velocity, m/s
u_{rms}	=	root mean square of velocity fluctuations, m/s
U_∞	=	free stream velocity, m/s
u_τ	=	wall-friction velocity, m/s
x, y, z	=	coordinate system placed at the plate leading edge, m
$\bar{x}$, $\bar{y}$, $\bar{z}$	=	coordinate system placed at the finlets trailing edge, m
ϕ	=	power spectral density, Pa^2/Hz
$\Lambda_{p,3}$	=	spanwise length scale, m
δ	=	boundary-layer thickness, m
δ^*	=	boundary-layer displacement thickness, m
γ_p^2	=	coherence of Surface pressure fluctuations
ν	=	kinematic viscosity, m^2/s
η_x, η_z	=	streamwise and spanwise separation distance between microphones, m
PSD	=	Power Spectral Density
SPL	=	Sound Pressure Level

I. Introduction

Airfoil self-noise is generated when the airfoil interacts with its own boundary layer and the near wake flow-field. Turbulent boundary layer trailing edge noise is one of the most important and common airfoil self-noise mechanisms [1] and various passive control methods, such as the trailing edge serrations [2, 3], trailing edge brushes [4], porous trailing edge [5-8], airfoil shape optimization [9], trailing edge morphing [10, 11] and recently upstream surface treatments [12-15], have been developed and tested over the past few years.

The use of microstructure surface treatments, known as the riblets, as a passive flow control method, has been the subject of much studies. Two-dimensional streamwise riblets have been widely investigated and shown to be effective in reducing the turbulent skin friction drag by as much as 10% [16]. Besides the 2D streamwise riblets, some studies have explored the effects of three-dimensional riblets such as the interlocking staggered riblets [17] and showed that 3D-riblets produce an appreciable drag reduction. However, the actual drag reduced using 3D riblets was less than that of equivalent 2D riblets.

Recently, Clark *et al.* [12, 18] studied the use of larger surface treatments, referred to as the finlets, for reducing the trailing-edge noise for a tripped DU96-W180 airfoil. The treatments were installed directly upstream of the trailing edge to modify the boundary layer prior to interacting with the trailing edge. Compared to the untreated airfoil, the treatments were found to be effective, providing a broadband farfield trailing-edge noise attenuation of up to 10dB. The aerodynamic analysis of Clark *et al.* [12, 18] also showed that the aerodynamic impact of the surface treatments is minimal, with the lift remained largely unaffected for almost the entire angle of attack range where finlets were found to be effective for reducing the trailing edge noise, and the drag coefficient showing slight increase, by an amount proportional to the increase in the wetted surface area associated with the treatments.

Afshari *et al.* [13] also studied the mechanisms responsible for the reduction of far-field noise using upstream surface treatments by simultaneous measurement of the surface pressure fluctuations and boundary layer velocity on a long flat-plate model, equipped with several streamwise and spanwise surface pressure microphones. It was shown that using finlets as a surface treatment can lead to around 8 dB reduction of the surface pressure fluctuations near the trailing edge. Furthermore, it was observed that the spanwise coherence can be significantly reduced over a wide range of frequencies.

Bodling *et al.* [15, 19] presented a numerical analysis of an airfoil geometry inspired by the down coat of the night owl. Their bioinspired geometry consisted of an array of finlets applied to the trailing edge region of the baseline airfoil and aligned in the flow direction. Their simulation results showed that the use of finlets can result in significant reduction in the unsteady surface pressure and farfield radiated noise, in agreement with the measurements available in the literature [12, 13]. Their results also revealed that the finlets treatment increase the distance between the boundary layer turbulence and the airfoil trailing edge and therefore reduce the trailing edge noise.

The work presented in this paper is a continuation of our earlier efforts on development of passive surface treatment based trailing edge noise control techniques [13]. In the present study, to improve the efficiency of the standard 2D

surface treatments, two different novel 3D surface treatment configurations have been introduced and tested. These novel complex configurations are shown to provide some improvement over the 2D finlet configurations, namely producing higher reduction in the surface pressure spectrum near the trailing edge, relatively smaller spanwise length scale of flow structures compared to the 2D treatments, lower eddy convection velocity and generally lower trailing edge noise, especially at mid to high frequency ranges. The experimental layout is described in section 2 and the main outcomes of the investigation are presented in section 3.

II.Experimental setup

The experiments were carried out in the blow-down subsonic wind tunnel of the Yazd University with a test-section size of 46 × 46 cm and length of 240 cm. The flat plate used in the present work has a chord length of 580 mm, a span of 456 mm and a thickness of 8 mm. The thickness of the trailing edge is t=0.4 mm, minimizing the possibility of trailing edge vortex shedding generation ($t/\delta^* < 0.3$) [20]. The experiments were carried out at zero angle of attack and at the free-stream velocity of 20 m/s, corresponding to the chord-based Reynolds number of $Re_c = 7.73 \times 10^5$. To ensure a fully turbulent boundary layer, the model was tripped at 5 percent of the chord-length, downstream of leading edge on the upper surface. The schematic of the flat plate model is shown in Fig. 1. Two coordinate systems have been used for describing the geometry and presenting the results. The (x, y, z) coordinate system placed at the leading edge of the flat plate is used for describing the finlets position and geometry, and the ($\bar{x}$, $\bar{y}$, $\bar{z}$) coordinate system, positioned at the trailing edge of the finlets, is used for presenting the flow and pressure results downstream of the treatment section, see Fig. 1.

To measure the unsteady surface pressure, a total number of 9 Knowles FG-23329-P07 miniature pressure transducers (p1-p9) are employed in the form of an L-shaped array on the upper surface of the plate, see Fig. 1. The locations of the pressure transducers on the upper surface of the flat plate are summarized in Table 1. A set of pressure transducers are distributed in the streamwise direction from x/c = 0.85 to 0.98 to provide information on the evolution of the boundary layer structures in the streamwise direction and the convection velocity of the turbulent eddies. Another set of microphones are positioned along the span of the plate at x/c=0.98 to provide information on the spanwise coherence and length scale of the boundary layer turbulent structures. The spanwise microphones are distributed with unequal separation distances, according to the potential function, $z/z_{min} = (z_{max}/z_{min})^{(i-2)/(N-2)}$, $i = 2..N$, in order to obtain a good range of distances with all pinhole pairs. The minimum and maximum lateral

distances of the pinholes from the flat plate midspan, z_{min} and z_{max}, are 3.2 mm and 40 mm, respectively. The transducers have a radius and height of 2.5 mm and a circular sensing area of 0.8 mm.

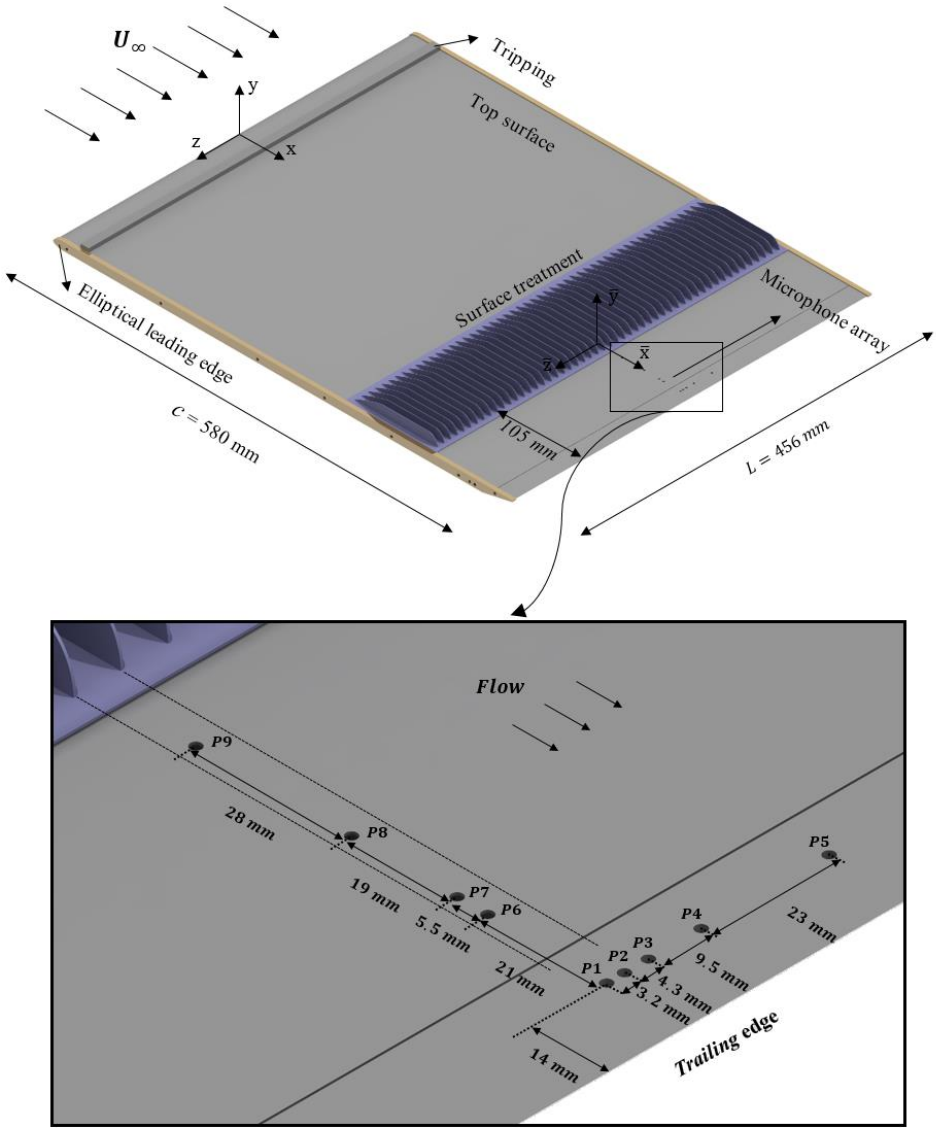

Fig. 1 The flat plate model used for the present study with an L-shaped pressure transducer array for the measurement of unsteady surface pressure near the trailing edge.

Table 1 Position of the unsteady pressure transducers on the upper surface of the flat plate.

Microphone number	Distance from TE (mm)	Distance from midspan (mm)
p1, p2, p3, p4, p5	14.0	0.0, 3.2, 7.5, 17.0, 40.0
p6, p7, p8, p9	35.0, 40.5, 59.5, 87.5	0.0

The microphones are embedded in the flat plate under a pinhole mask of 0.4 mm diameter in order to decrease the attenuation effects at high frequencies due to the finite size of the microphones sensing area [21, 22]. Due to the space constraints in the trailing edge area, two different techniques have been used for the installation of the FG pressure transducers. For the positions far from the trailing edge, the plate is thick enough to place the microphones vertically under the pinhole. For the positions near the trailing edge, the microphones have been installed inside the flat plate parallel to the surface (i.e. horizontally), linked to the pinhole via an L-shaped channel. A schematic of both arrangements is depicted in Fig. 2a.

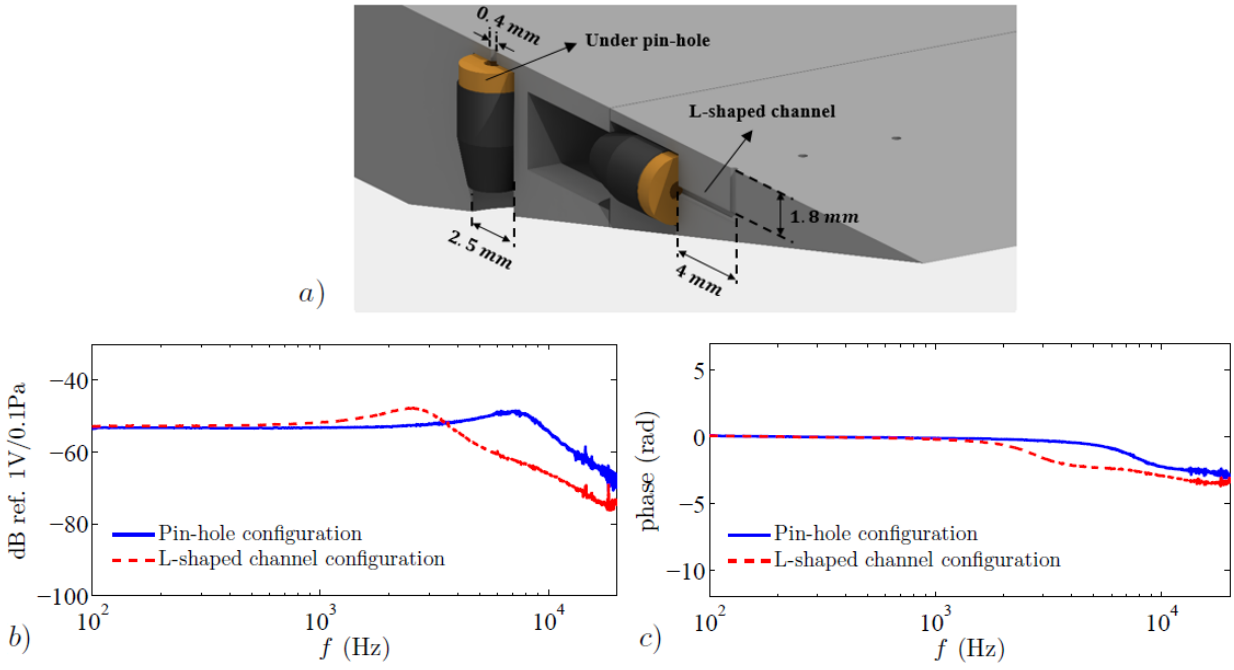

Fig. 2 (a) The pressure transducer installation near the trailing edge, (b, c) Amplitude and phase frequency response of a pressure transducer under the pin-hole configuration (p6) and with L-shaped channel configuration (p1).

A tube with a length of 110 mm and diameter of 10 mm along with a high-quality loudspeaker were used for the calibration of the microphones [23]. All microphones were calibrated in-situ with a white noise excitation signal over the frequency range of 100 Hz to 20 kHz, based on the calibration procedure proposed by Mish [24]. The amplitude and phase responses for both arrangements are presented in Figs. 2b and 2c, which show that both the pin-hole and L-shape channel methods can provide reliable data over the frequency range considered in this study. The attenuation

and possible resonances induced by the pinhole mask and the L-shaped channel are therefore accounted for by using this in-situ calibration. A more detailed explanation regarding the pressure transducers installation and calibration can be found in Ref. [25]. The microphones were powered by a 10-channel power module and the data were collected using a 16-channel NI PCI-6023E data acquisition system, at the sampling frequency of 40 kHz, for 20 seconds. Reliable and repeatable measurements are achieved for all microphones. The experimental uncertainty for the surface pressure spectra is mainly due to the statistical convergence error, which is inversely proportional to the number of records used [26]. To reduce such errors, in the present study, the spectra were calculated as the average of the spectra of individual data records obtained from dividing the pressure time series into a sequence of smaller records. The total number of records used was $N_r = 800$ resulting in an uncertainty of about 3.5%.

The boundary layer velocity measurements have been carried out using a single constant temperature hot-wire anemometer. The sensing element of the probe is a standard 5μm diameter tungsten wire with a length of 1.25 mm. The probe was calibrated using a standard Pitot tube located parallel to the incoming flow. Furthermore, the frequency response of the probe was verified by means of a square wave test to ensure a second-order response and demonstrating a 3 dB drop-off, based on the definition of Freymuth [27], at 30 kHz, for the free-stream mean velocity of 20 m/s. The probe is traversed in the boundary layer using a three-axis traverse unit controlled by stepper motors with 0.01 mm accuracy. The data were recorded at a sampling frequency of 40 kHz and for a sampling time of 10 seconds. To calculate the uncertainty of the hot-wire data, the methodology provided in Ref. [28] is used. The independent parameters such as the atmospheric temperature and pressure, curve fitting error in the calibration, A/D resolution uncertainty, probe positioning, and humidity are considered for the uncertainty analysis. Results revealed that the maximum uncertainty in the measured mean velocity and turbulence intensity are approximately 3%.

In the present study, blade-shaped fences (finlets) are chosen as the surface treatments for the flat plate. The design parameters of the various surface treatment configurations used in this study are illustrated in Fig. 3. The thickness of all finlets blades is 0.5 mm. Furthermore, the finlets have a height of $h = 12$ mm, corresponding to $h/\delta = 0.24$ or $h^+ = 624$ ($h^+ = hu_\tau/\nu$). The surface treatments are positioned at 105 mm upstream of the trailing edge and are placed such that the streamwise pressure transducers (p1, p6-p9) are located at the center channel made by finlet walls, see Fig. 1. The position of the spanwise transducers (p2-p4), relative to the finlet walls may vary depending on the finlet gap distance (s). Three types of finlet treatments will be examined here: (1) two uniformly placed two-dimensional surface treatments, with finlets spacings of $s = 8$ and 2 mm, corresponding to $s/\delta = 0.16, 0.04$ or $s^+ =$

416, 104 ($s^+ = su_\tau/\nu$). These finlet treatments will be referred to as the U-type s8 and s2 treatments, see Fig. 3a; (2) 3D interlocked staggered finlets, see Fig. 3b (referred to as the S-type finlets); and (3) finlets with gradually reduced spacing, see Fig. 3c (referred to as the G-type finlets). All the finlet treatments are fabricated using 3D rapid prototyping. The geometrical details of the U-, S- and G-type finlet treatments are provided in Fig. 3.

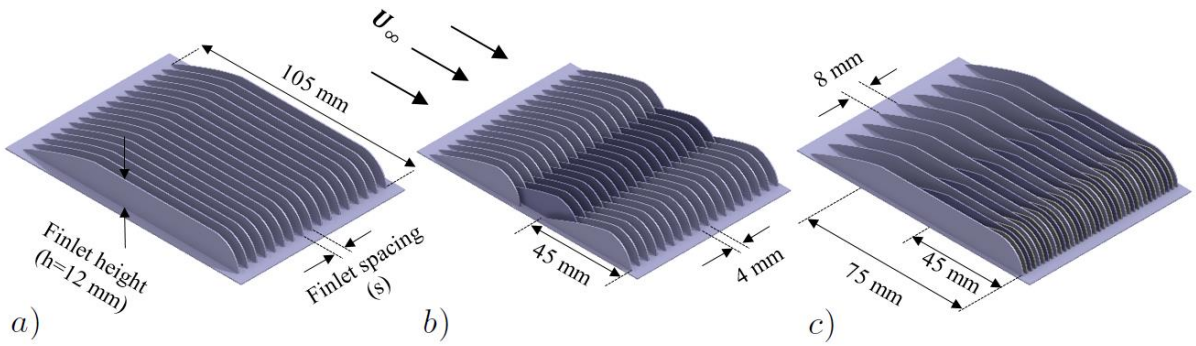

Fig. 3 Various surface treatment configurations, (a) uniformly placed 2D standard configuration (U-type), (b) staggered configuration (S-type), (c) gradually reduced spacing configuration (G-type).

III. Results and Discussion

A. Pressure Field

According to Amiet's [29] mathematical model, the wall pressure point spectrum, the frequency dependent spanwise length scale and the convection velocity of the surface pressure fluctuations in the vicinity of the trailing edge are the determining quantities for the prediction of the far-field trailing edge noise. Figure 4 presents the surface pressure power spectral density (PSD) measured by the pressure transducer p1 near the trailing edge (x/c=0.98) of the clean and treated flat plates, normalized by $p_{ref} = 20\ \mu Pa$. The unsteady pressure data are corrected according to the calibration procedure described in [24] and the Corcos' correction [21]. As shown, the surface pressure PSD curve for the clean flat plate case follows decay rates of f^{-1} and f^{-5} at mid and high frequencies, which agrees with the results reported in the literature [20, 30]. As can be seen, the U-type finlets with coarse and fine spacing (s=8 mm and 2 mm) exhibit very different surface pressure behavior at the trailing edge. For the finlets with coarse spacing (s8), the presence of the upstream surface treatment has led to a significant reduction of the surface pressure PSD over the mid to high frequency ranges, with no noticeable changes to the low frequency energy content of the boundary layer. For

the surface treatment with fine spacing (s2), results demonstrate that while the presence of the upstream surface treatment leads to a greater reduction in the pressure PSD at high frequencies, it also results in a significant increase in the energy content of the surface pressure at low frequencies. These trends are consistent with the far-field noise observations of Clark *et al*. [12] which showed that reducing the spacing between the finlets can result in low frequency increase of the far-field trailing-edge noise. As can be seen in Fig. 4, for the U-type finlets with fine spacing (s2), the spectral broadband peak occurs at about 130 Hz, corresponding to $fh/U_\infty = 0.078$, where h is the finlets height. This also matches well with the non-dimensional vortex shedding frequency in the wake of backward facing steps (BFS) [31, 32]. Finally, the results for the S-type and G-type finlets have shown that they can provide a better performance than both the U-type s2 and s8 treatments at high frequencies and have less negative impact at low frequencies than the s2 treatment. This is an interesting observation which means that the more geometrically complex finlet treatments are able to increase the energy decay at high frequencies, and that the low frequency hump is somewhat controlled. The mechanisms through which the low frequency PSD is reduced, relative to the U-type s2, will be discussed in Section III.B.

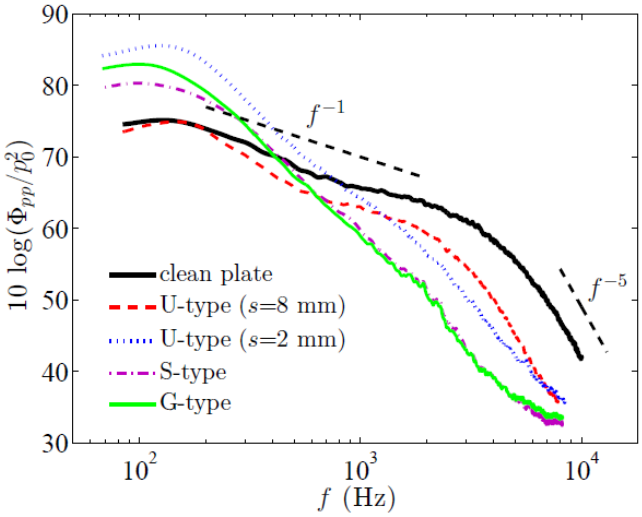

Fig. 4 Surface pressure power spectral density referenced to p_{ref} =20 μPa measured by microphone p1 on the trailing edge of the clean and treated flat plates.

To investigate the effect of the finlets on the unsteady surface pressure in the spanwise direction and the potential three-dimensionality effect of the finlets, the pressure power spectral density results obtained from all the spanwise

microphones (p1-p5) for the different treated flat plates are provided in Fig. 5. These pressure transducer locations cover a wide enough spatial range, relative to the finlets walls, to demonstrate any three-dimensionality effects. In all sub-plots, z/h=0 corresponds to the center-point of the finlet channels. The exact location of each pressure transducer can also be found from Table 1. As can be seen, the surface pressure PSD results remain almost unchanged, particularly at low and mid frequencies, regardless of the relative spanwise location of the pressure transducers and the finlet walls. At the high frequencies, the PSD results again show a good collapse with a maximum deviation of 4dB in the case of the s8 treatment and 2dB for the other cases. The pressure PSD results at different spanwise locations, therefore, suggest that the pressure field at flat plate trailing edge region is nearly statistically stationary in the spanwise direction for all surface treatments.

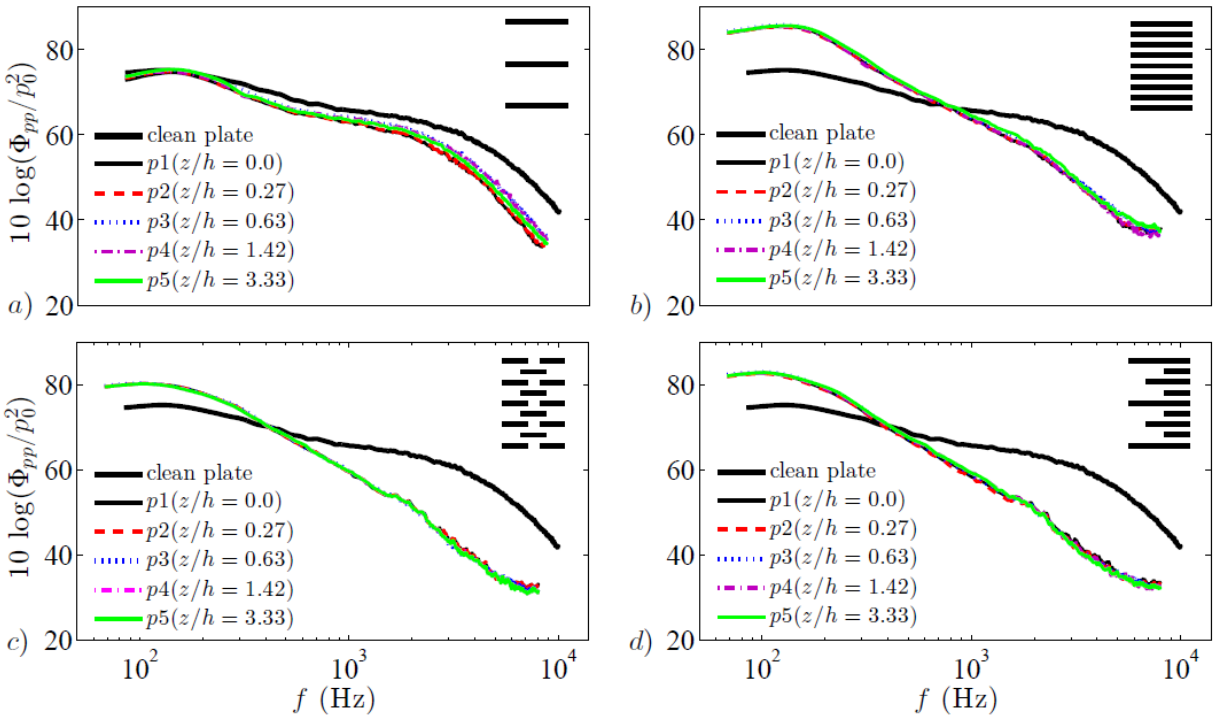

Fig. 5 Surface pressure power spectral density measured by various spanwise microphones (p1-p5) at the trailing edge of the treated flat plates, (a) U-type (s=8 mm), (b) U-type (s=2 mm), (c) S-type, (d) G-type.

The effects of the presence of the finlets on the lateral coherence of the boundary layer structures, obtained using the p1 to p5 pressure transducers, located at x/c=0.98 are presented in Fig. 6. The results in this figure show the changes to the lateral coherence, *i.e.* $\Delta\gamma^2 = \gamma^2_{treated} - \gamma^2_{clean}$, as a function of separation distance (η_z) and frequency.

Results show that the use of the coarse U-type surface treatment (s8) leads to an increase in the lateral coherence at low to mid frequencies without any significant changes at high frequencies, Fig. 6a. The results for the U-type finlets with fine spacing (s2), on the other hand, shows that the use of such finely distributed finlets can somewhat reduce the coherence at mid frequencies with an undesirable increase at low frequencies, see Fig. 6b. As can be seen, the lateral coherence of the boundary layer structures for both proposed 3D surface treatments, especially the G-type case, is fairly similar to the s2 treatment case, see Figs. 6c and 6d. The spanwise length-scale of the surface pressure fluctuations, $\Lambda_{p,3}(f)$, was calculated using the spanwise coherence, $\gamma^2_{p_i,p_j}(f,\eta_z)$, measured using the p1 to p5 pressure transducers at $x/c = 0.98$ ($\Lambda_{p,3}(f) = \int_0^\infty \gamma_{p,ij}(f,\eta_z)d\eta_z$). Figure 7 shows the effects of the finlets presence on the spanwise length-scale. Results show that using both the fine (s2) and coarse (s8) U-type finlets leads to an undesirable increase in the spanwise length-scale at low to mid frequencies. As seen in Fig 7, the proposed 3D surface treatments cause a smaller increase in the spanwise length-scale at low frequencies compared to the standard U-type treatments, particularly the U-type s8 treatment. This implies that in the presence of the proposed 3D surface treatments, the flow structures passing over the trailing edge are less prone to cause high level of noise compared to the U-type treatment.

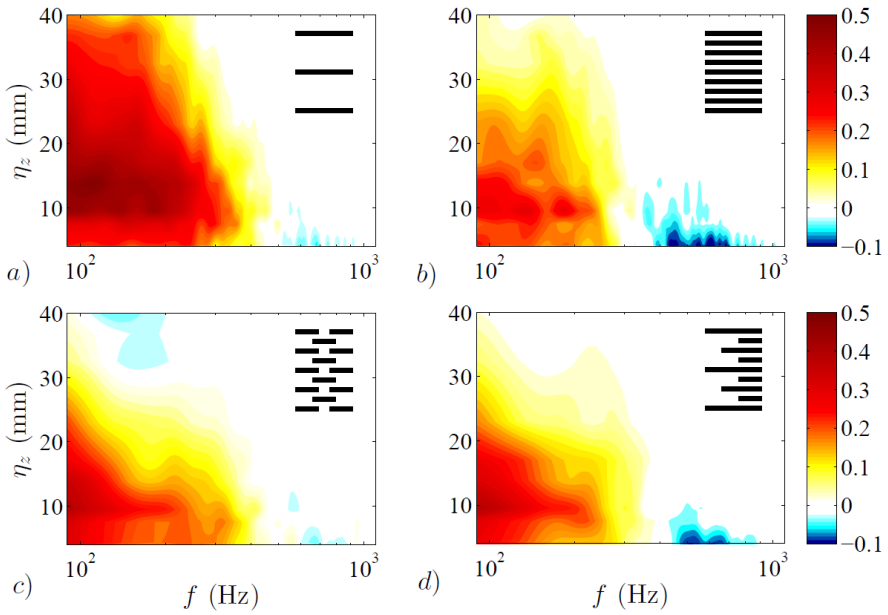

Fig. 6 Changes in the lateral coherence, $\Delta\gamma^2 = \gamma^2_{treated} - \gamma^2_{clean}$, measured between spanwise microphones for different finlet treatments, (a) U-type (s=8 mm), (b) U-type (s=2 mm), (c) S-type, (d) G-type.

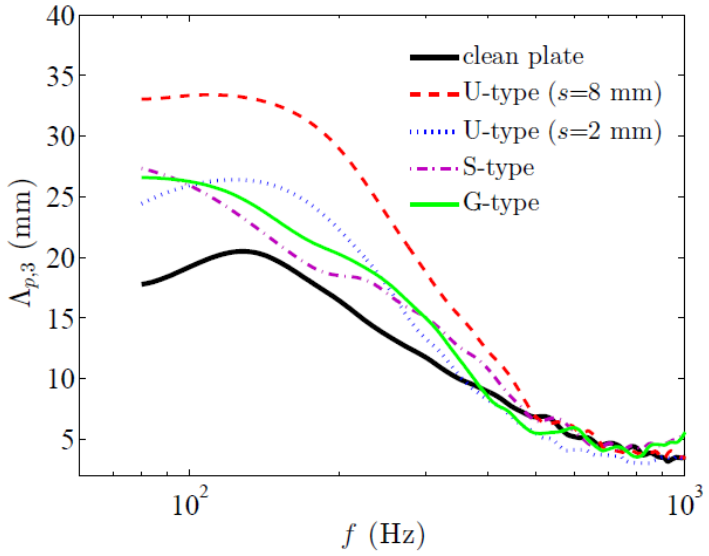

Fig. 7 Spanwise length scale ($\Lambda_{p,3}$) measured at x/c=0.98 for the clean and treated flat plates.

The convection velocity of the wall fluctuating pressure field is defined using the phase shift calculated from the cross-spectra of two streamwise pressure transducers, as explained in Ref. [13]. Table 2 summarizes the values of the convection velocity of the boundary layer structures, calculated using the phase analysis between the microphones p6 and p7 (η_x=5.5 mm) near the trailing edge for the clean and treated cases. It is clear from the results that the presence of the surface treatments generally leads to a reduction in the convection velocity in the trailing edge region. Results have also shown that the s2 type causes significant reduction in the convection velocity compared to the s8 type and that the novel 3D treatments have a fairly similar behavior to the s2 type finlets.

Table 2 Convection velocity calculated from the phase shift between microphones p6 and p7 (η_x=5.5 mm).

Configuration	Clean plate	U-type (s=8 mm)	U-type (s=2 mm)	S-type	G-type
U_C/U_∞	0.6	0.46	0.25	0.26	0.24

B. Boundary Layer Velocity Field

To gain a better insight into the mechanisms through which the proposed 3D surface treatments affect the flow structures and improve the efficiency of the standard 2D surface treatments, the boundary layer flow field downstream of the clean and treated flat plates, measured along the centerline of the finlet channels (i.e. along the $\bar{z} = 0$ axis), are

studied. In Fig. 8, the contour maps of the dimensionless mean velocity and the turbulence intensity (u_{rms}/U_∞) downstream of the two- and three-dimensional surface treatments are presented and compared against the clean flat plate results. Figures 8c and 8d show that the use of U-type finlets with coarse spacing (s8) leads to the reduction of both the mean velocity and turbulence intensity in the near wall region downstream of the finlets compared to the clean plate case. It may be hypothesized that in the case of coarse U-type surface treatment (s8), significant portion of the boundary layer flow (up to approximately 25% of the boundary layer thickness, $y/\delta \leq 0.25$) is channeled between the finlets, leading to an increased wetted surface area and therefore possible increase in energy dissipation via surface friction.

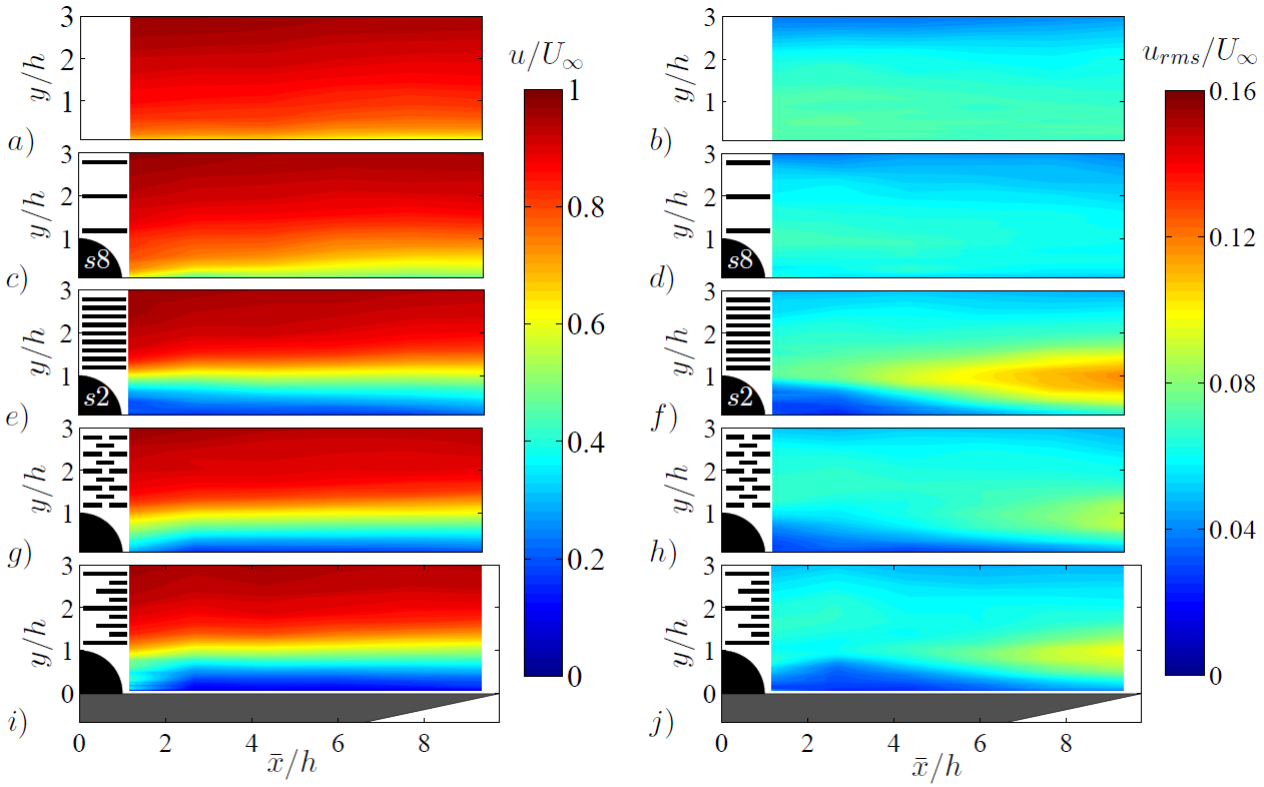

Fig. 8 Turbulence intensity contour map downstream of the different surface treatments. (a, b) Clean flat plate, (c, d) U-type (s=8 mm) finlets, (e, f) U-type (s=2 mm) finlets, (g, h) S-type finlets, (i, j) G-type finlets.

The contour map of the mean velocity and turbulence intensity downstream of the fine U-type s2 case, Figs. 8e and 8f, shows the emergence of a shear layer at about $y/h \approx 1$ which extends downstream to the reattachment point at about $\bar{x}/h \approx 9$. The behavior observed here is similar to the flow-field behind a backward-facing step [33, 34]. It

can, therefore, be concluded that by reducing the spacing between finlets (from 8 mm to 2 mm), some parts of the upstream flow separate at the end corner of the finlets and forms a free-shear layer downstream of the finlets. Finally, the contour maps of the turbulence intensity downstream of the 3D surface treatments, Figs. 8h and 8j, show that although the presence of the 3D surface treatments can lead to flow separation and formation of a shear layer downstream of the finlets, this shear layer, especially for the S-type case, is much weaker than the U-type s2 treatment case.

To better understand the flow behavior downstream of the U-type and novel 3D surface treatments, the boundary layer mean velocity (u/U_∞) and the turbulence intensity (u_{rms}/U_∞) profiles, measured at the location of the p1 pressure transducer, *i.e.* x/c=0.98 and at the middle of the space made by finlet walls, are studied. Results in Fig. 9 show that all two- and three-dimensional surface treatments create a velocity deficit in the near wall region, $y/h < 2$, indicating significant changes to the boundary layer structures downstream of the finlet treatments, Fig 9a. As seen, the changes in the boundary layer mean velocity deficit increases with decreasing the spacing between the finlets of the U-type treatment from 8 mm to 2 mm. Furthermore, the boundary layer mean velocity profiles downstream of both the 3D cases are similar to the profile of the fine U-type surface treatment (s2), which is consistent with the eddy convection velocity results in the vicinity of the flat plate trailing edge, see Table 2. As can be seen in Fig. 9b, in the presence of the U-type finlets with coarse spacing (s8), the passage of the flow through the treatment channels lead to a reduction in the turbulent intensity profile within $0 \leq y/h \leq 2.5$. Furthermore, reducing the finlets spacing from 8 mm to 2 mm leads to a strong rms velocity peak at $y/h \approx 1$, which is due to the turbulence generated by a shear layer originating from the top surface of the finlets, as shown in Fig. 8f. Interestingly, results show that using both proposed 3D surface treatments create a lower rms velocity peak at $y/h \approx 1$ than the s2 case and leads to a more pronounced reduction of the turbulence intensity in the near wall region than both the s2 and s8 finlets. This behavior is consistent with the reduction of the undesirable low frequency content of the surface pressure PSD, achieved by replacing the U-type fine finlets with 3D surface treatments, as observed in Fig 4.

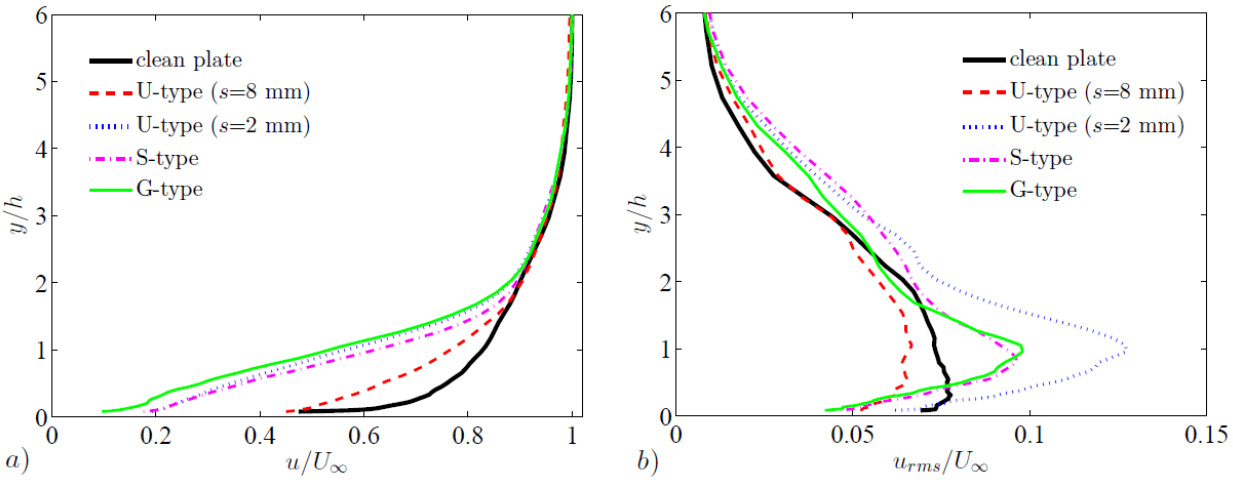

Fig. 9 (a) Boundary layer mean velocity profiles, (b) Turbulence intensity profiles at the position of microphone p1 (x/c = 0.98) for the clean and treated flat plates.

The results presented in Fig. 10 show the velocity PSD contour plots, normalized by the results of the clean flat plate ($\Delta\phi_{uu} = 10log_{10}(\phi_{uu,treated}/\phi_{uu,clean})$). The results in Fig. 10a, show that the use of the s8 finlets leads to the reduction of the low frequency energy content of the boundary layer structures over the normal distance from the plate of $y/h < 3$. Furthermore, it can be observed that the energy content of the near the wall mid- to high-frequency structures has been reduced. The normalized velocity PSD results for the U-type s2 finlets is presented in Fig. 10b. As can be seen, the turbulence energy content of the near the wall structures at mid- to high-frequencies are reduced, even more than that observed for the coarse U-type finlets (s8). However, in the region between $0.5< y/h < 2$, the turbulence energy content of the flow is significantly increased, particularly at low frequencies, due to the additional turbulence generated in the shear layer originating from the flow separation formed at the end of the finlets [35], as also evidenced by the mean velocity gradients in Fig. 9a and the turbulence intensity peaks in Fig. 9b. Therefore, for the fine finlet treatment, the flow separation and emergence of the high energy region are believed to be responsible for the undesirable low frequency increase in the pressure PSD. Results presented in Figs. 10c and 10d show that the presence of both the 3D surface treatments leads to more reduction in the energy content of near the wall mid- to high-frequency structures than the U-type coarse and fine finlets. Furthermore, the aforementioned undesirable increase in the turbulence energy content of the flow is decreased due to the presence of a weaker shear layer downstream of the proposed 3D surface treatments, especially for the S-type configuration. This is in agreement with the surface pressure

PSD observations which show that both the proposed 3D surface treatments are more effective in reducing the pressure PSD at mid- to high-frequencies with lower pressure PSD increase at low frequencies than the 2D surface treatments.

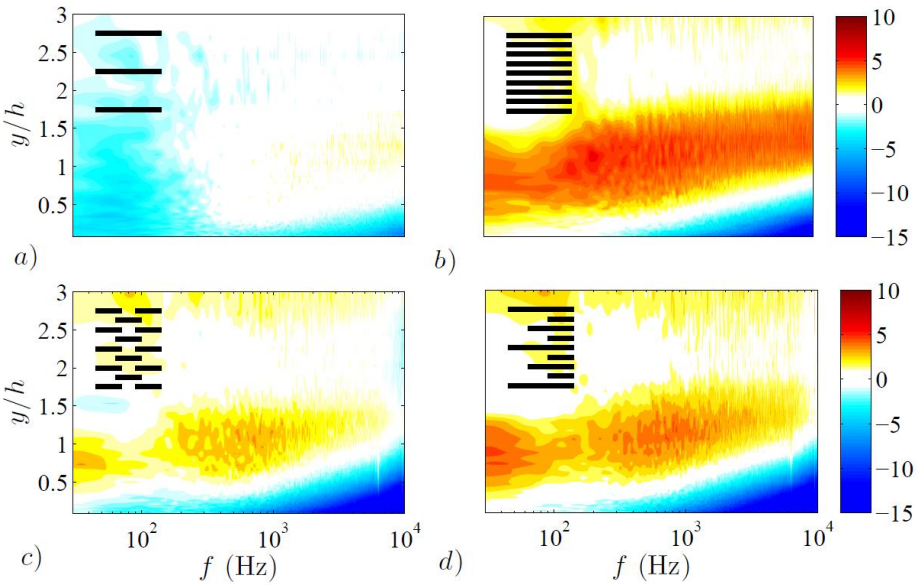

Fig. 10 Normalized velocity power spectral density, $10log_{10}(\phi_{uu,treated}/\phi_{uu,clean})$, contour plots for treated flat plates near the trailing edge at x/c = 0.98, (a) U-type (s=8 mm), (b) U-type (s=2 mm), (c) S-type, (d) G-type.

Finally, the drag coefficient (C_D) for the clean and treated flat plates can be estimated using a momentum balance approach using the boundary layer velocity data [6, 36]. The drag coefficient can be estimated using,

$$C_D = \frac{2}{c}\int \frac{u}{U_\infty}\left(1-\frac{u}{U_\infty}\right)dy + \frac{2}{c}\int \left(\frac{u_{rms}}{U_\infty}\right)^2 dy. \quad (1)$$

It should be noted that since the finlets are only placed on the top surface of the plate, the drag estimate analysis is also performed only for the plate top surface. Using the velocity and rms velocity data obtained from the hotwire measurements, the drag coefficient for the clean case was found to be approximately 0.0167, while that for the U-type s8, U-type s2, were found to be 0.0182, 0.0220, and for the S-type and G-type treatments 0.0206 and 0.0201, respectively. Our aerodynamic analysis of the flat plate fitted with finlets has, therefore, shown that the use of surface treatments can lead to an increase in the drag coefficient, which is likely to be due to the increase in wetted surface area of the plate. This is consistent with the prior observations by Clark *et al.* [12]. Furthermore, while the U-type s8

finlets is observed to cause the least drag increase compared to the clean case, results have also shown that the 3D S-type and G-type finlets produce less drag than the U-type s2.

The above results have shown that the finlets wake region is characterized by the interaction between a lower layer of relatively low velocity air and a region of higher velocity wind flowing above the finlets. Because of the finlets finite porosity, the structure of turbulence downstream of the finlets experiences both flow types and therefore it can be said that the flow behind the finlets is a superposition of 'leakage flow' and BFS-like flow, with their relative importance determined by the finlets spacing, i.e. large finlet spacing with large leakage flow contribution and small finlet spacing with large BFS-like flow contribution. On the other hand, the boundary layer flow measurements downstream of the three-dimensional surface treatments revealed that the complex 3D surface treatments can reduce the flow separation and the formation of a shear layer downstream of the finlets.

C. Trailing Edge Noise

To compare trailing-edge noise reduction capability of the proposed 3D finlets against the 2D U-type surface treatments, an extension of the Amiet's original formulation of trailing-edge noise, given by Roger *et al*. [37], has been used to evaluate the changes in the radiated sound levels due to the presence of the finlets. The changes in predicted noise levels are plotted in Fig. 11. It should be noted that spanwise length scale, required in the Amiet's model, was calculated by performing an integration of the surface pressure cross-spectra over the span length, as $\Lambda_{p,3}(f) = \int_0^\infty \gamma_{p,ij}(f,\eta_z)d\eta_z$. At higher frequencies, where the surface pressure signal coherence level drops, the spanwise length-scale can be estimated using Amiet's empirical relation $\Lambda_{p,3}(\omega) = aU_c/\omega$ [29], where a is a constant and can be found to give the best fit, ranging from 1.8 to 3.7 for different cases in this study. The process of calculating the spanwise length scale at low and high-frequencies is explained in Ref. [38].

All treatments are found to be effective at mid to high frequencies. However, the treatments appear to increase the trailing edge noise at the low frequencies. As can be seen, the use of U-type finlets with coarse spacing (s8) leads to a significant noise reduction at high frequencies (up to 11 dB at 8 kHz) with approximately 2.5 dB increase at low frequencies ($f < 300$ Hz). For the surface treatment with fine spacing (s2), these effects have been observed to intensify, i.e. more increase at low frequencies (up to 9 dB) and more reduction at high frequencies (up to 19 dB at about 5 kHz). Finally, the predicted trailing edge noise results for the S-type and G-type finlets have shown that proposed 3D surface treatments, can create more noise reduction than the 2D finlet configurations at high frequencies

(up to 25 dB at about 5 kHz) with a comparable low frequency negative impact of the s8 treatment, especially for the S-type case.

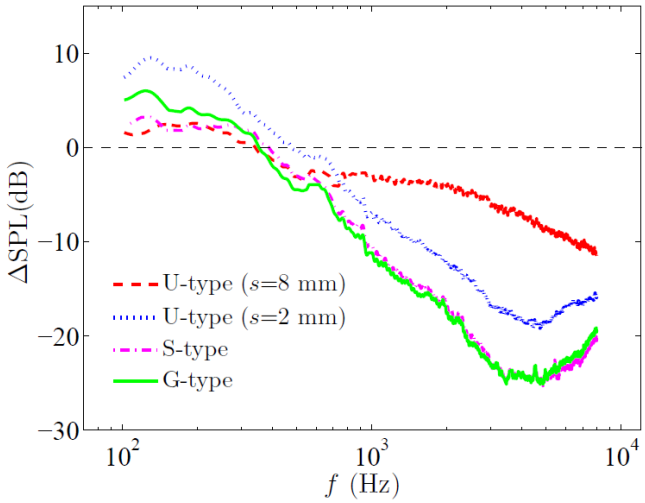

Fig. 11 The changes in the trailing-edge noise level estimated using Amiet's model, based on the pressure data collected from the trailing-edge microphones.

IV. Conclusion

The current work is concerned with the application of two- and three-dimensional surface treatments positioned upstream of the trailing edge of a flat plate for the suppression of the trailing edge noise at source. To demonstrate the capabilities of the proposed novel trailing edge noise control technique, a long flat-plate model, equipped with several streamwise and spanwise surface pressure microphones, has been designed and built. Results have shown that the efficiency of the standard two-dimensional surface treatments in reducing the surface pressure power spectral density, the spanwise length scale and the eddy convection velocity is strongly dependent on the finlets spacing. It has also been shown that the proposed three-dimensional surface treatments can deliver a better performance than the straight two-dimensional ones in reducing trailing edge noise especially at high frequencies. Finally, the boundary layer flow measurements downstream of the surface treatments revealed that three-dimensional surface treatments may reduce the flow separation and formation of a shear layer downstream of the finlets, which can improve the performance of the surface treatment for suppression of the trailing edge noise at source.

Acknowledgments

The second author (MA) would like to acknowledge the financial support of the Royal Academy of Engineering.

References

[1] Brooks, T. F., Pope, D. S., and Marcolini, M. A. Airfoil self-noise and prediction: National Aeronautics and Space Administration, Office of Management, Scientific and Technical Information Division, 1989.

[2] Lyu, B., Azarpeyvand, M., and Sinayoko, S. "Prediction of noise from serrated trailing edges," Journal of Fluid Mechanics Vol. 793, 2016, pp. 556-588.
doi: 10.1017/jfm.2016.132

[3] Liu, X., Kamliya Jawahar, H., Azarpeyvand, M., and Theunissen, R. "Aerodynamic performance and wake development of airfoils with serrated trailing-edges," AIAA Journal, 2017, pp. 3669-3680.
doi: 10.2514/1.J055817

[4] Finez, A., Jondeau, E., Roger, M., and Jacob, M. C. "Broadband noise reduction with trailing edge brushes," 16th AIAA/CEAS Aeroacoustics Conference. Stockholm, Sweden, 2010, p. 3980.
doi: 10.2514/6.2010-3980

[5] Geyer, T., Sarradj, E., and Fritzsche, C. "Measurement of the noise generation at the trailing edge of porous airfoils," Experiments in Fluids Vol. 48, No. 2, 2009, pp. 291-308.
doi: 10.1007/s00348-009-0739-x

[6] Ali, S. A. S., Azarpeyvand, M., and da Silva, C. R. I. "Trailing-edge flow and noise control using porous treatments," Journal of Fluid Mechanics Vol. 850, 2018, pp. 83-119.
doi: 10.1017/jfm.2018.430

[7] Showkat Ali, S. A., Azarpeyvand, M., Szőke, M., and Ilário da Silva, C. R. "Boundary layer flow interaction with a permeable wall," Physics of Fluids Vol. 30, No. 8, 2018, p. 085111.
doi: 10.1063/1.5043276

[8] Showkat Ali, S. A., Szoke, M., Azarpeyvand, M., and Ilário, C. "Trailing Edge Bluntness Flow and Noise Control Using Porous Treatments," 22nd AIAA/CEAS Aeroacoustics Conference. Lyon, France, 2016, p. 2832.
doi: 10.2514/6.2016-2832

[9] Oerlemans, S., Fisher, M., Maeder, T., and Kögler, K. "Reduction of wind turbine noise using optimized airfoils and trailing-edge serrations," AIAA journal Vol. 47, No. 6, 2009, pp. 1470-1481.
doi: 10.2514/1.38888

[10] Jawahar, H. K., Ai, Q., and Azarpeyvand, M. "Experimental and numerical investigation of aerodynamic performance for airfoils with morphed trailing edges," Renewable Energy Vol. 127, 2018, pp. 355-367.
doi: 10.1016/j.renene.2018.04.066

[11] Ai, Q., Weaver, P. M., and Azarpeyvand, M. "Design and mechanical testing of a variable stiffness morphing trailing edge flap," Journal of Intelligent Material Systems and Structures Vol. 29, No. 4, 2018, pp. 669-683.
doi: 10.1177/1045389X17721028

[12] Clark, I. A., Alexander, W. N., Devenport, W., Glegg, S., Jaworski, J. W., Daly, C., and Peake, N. "Bioinspired trailing-edge noise control," AIAA Journal Vol. 55, No. 3, 2017, pp. 740-754.
doi: 10.2514/1.J055243

[13] Afshari, A., Azarpeyvand, M., Dehghan, A. A., and Szőke, M. "Trailing Edge Noise Reduction Using Novel Surface Treatments," 22nd AIAA/CEAS Aeroacoustics Conference. Lyon, France, 2016, p. 2834.
doi: 10.2514/6.2016-2834

[14] Afshari, A., Dehghan, A. A., Azarpeyvand, M., and Szőke, M. "Three-dimentional surface treatments for trailing edge noise reduction," 23rd International Congress on Sound and Vibration, ICSV. 2016.

[15] Bodling, A., and Sharma, A. "Numerical investigation of noise reduction mechanisms in a bio-inspired airfoil," Journal of Sound and Vibration, 2019.
doi: 10.1016/j.jsv.2019.02.004

[16] Bechert, D., Bruse, M., Hage, W., Van der Hoeven, J. T., and Hoppe, G. "Experiments on drag-reducing surfaces and their optimization with an adjustable geometry," Journal of fluid mechanics Vol. 338, 1997, pp. 59-87.
doi: 10.1017/S0022112096004673

[17] Bechert, D., Bruse, M., and Hage, W. "Experiments with three-dimensional riblets as an idealized model of shark skin," Experiments in fluids Vol. 28, No. 5, 2000, pp. 403-412.
doi: 10.1007/s003480050400

[18] Clark, I., Baker, D., Alexander, W. N., Devenport, W. J., Glegg, S. A., Jaworski, J., and Peake, N. "Experimental and theoretical analysis of bio-inspired trailing edge noise control devices," 22nd AIAA/CEAS Aeroacoustics Conference. Lyon, France, 2016, p. 3020.
doi: 10.2514/6.2016-3020

[19] Bodling, A., and Sharma, A. "Numerical investigation of low-noise airfoils inspired by the down coat of owls," Bioinspiration & biomimetics Vol. 14, No. 1, 2018, p. 016013.
doi: 10.1088/1748-3190/aaf19c

[20] Blake, W. "Mechanics of flow-induced sound and vibration. Volume 1 General concepts and elementary source. Volume 2-Complex flow-structure interactions," Aplikace Matematiky, Applied Mathematics Vol. 17, 1986.

[21] Corcos, G. "Resolution of pressure in turbulence," The Journal of the Acoustical Society of America Vol. 35, No. 2, 1963, pp. 192-199.
doi: 10.1121/1.1918431

[22] Willmarth, W., and Roos, F. "Resolution and structure of the wall pressure field beneath a turbulent boundary layer," Journal of Fluid Mechanics Vol. 22, No. 01, 1965, pp. 81-94.
doi: 10.1017/S0022112065000599

[23] Maryami, R., Azarpeyvand, M., Dehghan, A., and Afshari, A. "An Experimental Investigation of the Surface Pressure Fluctuations for Round Cylinders," Journal of Fluids Engineering Vol. 141, No. 6, 2019, p. 061203.
doi: 10.1115/1.4042036

[24] Mish, P. F. "Mean loading and turbulence scale effects on the surface pressure fluctuations occurring on a NACA 0015 airfoil immersed in grid generated turbulence." M.S. Thesis, Virginia Polytechnic Institute and State University, 2001.

[25] Afshari, A., Azarpeyvand, M., Dehghan, A. A., and Szoke, M. "Effects of Streamwise Surface Treatments on Trailing Edge Noise Reduction," 23rd AIAA/CEAS Aeroacoustics Conference. 2017, p. 3499.
doi: 10.2514/6.2017-3499

[26] Bendat, J. S., and Piersol, A. G. Random data: analysis and measurement procedures: John Wiley & Sons, 2011.

[27] Freymuth, P. "Feedback Control Theory for Constant-Temperature Hot-Wire Anemometers," Review of Scientific Instruments Vol. 38, No. 5, 1967, pp. 677-681.
doi: 10.1063/1.1720798

[28] Yavuzkurt, S. "A guide to uncertainty analysis of hot-wire data," ASME, Transactions, Journal of Fluids Engineering Vol. 106, 1984, pp. 181-186.
doi:10.1115/1.3243096

[29] Amiet, R. "Noise due to turbulent flow past a trailing edge," Journal of sound and vibration Vol. 47, No. 3, 1976, pp. 387-393.
doi: 10.1016/0022-460X(76)90948-2

[30] Hwang, Y. F., Bonness, W. K., and Hambric, S. A. "Comparison of semi-empirical models for turbulent boundary layer wall pressure spectra," Journal of Sound and Vibration Vol. 319, No. 1-2, 2009, pp. 199-217.
doi: 10.1016/j.jsv.2008.06.002

[31] Lee, I., and Sung, H. "Characteristics of wall pressure fluctuations in separated and reattaching flows over a backward-facing step: Part I. Time-mean statistics and cross-spectral analyses," Experiments in Fluids Vol. 30, No. 3, 2001, pp. 262-272.

doi: 10.1007/s003480000172

[32] Liu, Y. Z., Kang, W., and Sung, H. J. "Assessment of the organization of a turbulent separated and reattaching flow by measuring wall pressure fluctuations," Experiments in Fluids Vol. 38, No. 4, 2005, pp. 485-493.
doi: 10.1007/s00348-005-0929-0

[33] Bradshaw, P., and Wong, F. "The reattachment and relaxation of a turbulent shear layer," Journal of Fluid Mechanics Vol. 52, No. 01, 1972, pp. 113-135.
doi: 10.1017/S002211207200299X

[34] Eaton, J., and Johnston, J. "A review of research on subsonic turbulent flow reattachment," AIAA J Vol. 19, No. 9, 1981, pp. 1093-1100.
doi: 10.2514/3.60048

[35] Ji, M., and Wang, M. "Aeroacoustics of turbulent boundary-layer flow over small steps," 48th AIAA aerospace sciences meeting including the new horizons forum and aerospace exposition. Orlando, Florida, 2010, p. 6.
doi: 10.2514/MASM10

[36] Naghib-Lahouti, A., Hangan, H., and Lavoie, P. "Distributed forcing flow control in the wake of a blunt trailing edge profiled body using plasma actuators," Physics of Fluids Vol. 27, No. 3, 2015, p. 035110.
doi: 10.1063/1.4914406

[37] Roger, M., Moreau, S., and Wang, M. "An analytical model for predicting airfoil self-noise using wall-pressure statistics," Annual Research Brief, Center for Turbulence Research, Stanford University, 2002, pp. 405-414.

[38] Clark, I. A. "Bio-Inspired Control of Roughness and Trailing Edge Noise." Vol. PhD thesis, Virginia Tech, 2017.